NANO LETTERS

Letter

pubs.acs.org/NanoLett

Colloidal Quantum Dot Photovoltaics: The Effect of Polydispersity

David Zhitomirsky,[†,§] Illan J. Kramer,[†,§] André J. Labelle,[†] Armin Fischer,[†] Ratan Debnath,[†] Jun Pan,[‡] Osman M. Bakr,[‡] and Edward H. Sargent*[,†]

[†]Department of Electrical and Computer Engineering, University of Toronto, 10 King's College Road, Toronto, Ontario M5S 3G4, Canada

[‡]Division of Physical Sciences and Engineering, Solar and Photo-voltaics Engineering Center, King Abdullah University of Science and Technology (KAUST), Thuwal 23955- 6900, Saudi Arabia

Supporting Information

ABSTRACT: The size-effect tunability of colloidal quantum dots enables facile engineering of the bandgap at the time of nanoparticle synthesis. The dependence of effective bandgap on nanoparticle size also presents a challenge if the size dispersion, hence bandgap variability, is not well-controlled within a given quantum dot solid. The impact of this polydispersity is well-studied in luminescent devices as well as in unipolar electronic transport; however, the requirements on monodispersity have yet to be quantified in photovoltaics. Here we carry out a series of combined experimental and model-based studies aimed at clarifying, and quantifying, the importance of quantum dot monodispersity in photovoltaics. We successfully predict, using a simple model, the dependence of both open-circuit voltage and photoluminescence behavior on the density of small-bandgap (large-diameter) quantum dot inclusions. The model requires inclusion of trap states to explain the experimental data quantitatively. We then explore using this same experimentally tested model the implications of a broadened quantum dot population on device performance. We report that present-day colloidal quantum dot photovoltaic devices with typical inhomogeneous linewidths of 100−150 meV are dominated by surface traps, and it is for this reason that they see marginal benefit from reduction in polydispersity. Upon eliminating surface traps, achieving inhomogeneous broadening of 50 meV or less will lead to device performance that sees very little deleterious impact from polydispersity.

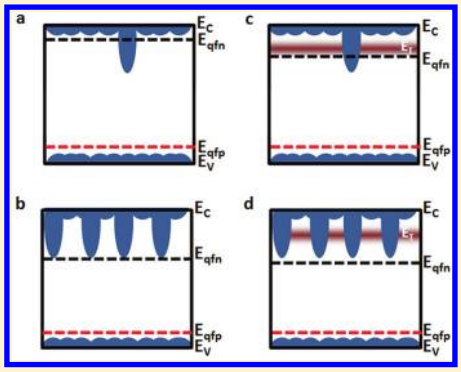

KEYWORDS: *Energy landscaping, colloidal quantum dot, photovoltaics, solar cell, polydispersity, bandgap engineering*

Colloidal quantum dots (CQDs) are nanoparticles, synthesized and suspended in solution, whose tunable dimensions dictate their optical and electrical properties.[1] These materials have been successfully employed as the active layer in optoelectronic devices such as photodetectors,[2,3] light emitting diodes,[4,5] and solar cells.[6,7] At present, the most efficient CQD solar cells[8] employ the depleted heterojunction architecture consisting of a p-type PbS CQD layer coating a transparent n-type metal oxide.[9] Within these architectures, the PbS film is often idealized as having substantially uniform electronic properties with a single, well-defined effective quantum-confined bandgap.

In fact, a population of CQDs has some finite distribution of dot diameters, hence a variance in the quantum-confined bandgap of the dots in this population, characterized as inhomogeneous broadening. In light-emitting and lasing devices, polydispersity widens the emission and gain bandwidths, respectively.[10,11] In electronic devices such as field-effect transistors, electronic transport can be enhanced through the use of highly monodispersed quantum dots, enabling dense packing and, potentially, superlattice-based delocalized transport.[12,13]

The need for control over CQD population inhomogeneous broadening is thus widely recognized in the CQD community; and rapid nucleation and growth, followed by size-selective precipitation, are available to narrow this distribution.[14]

Here we investigate the importance of monodispersity in the specific context of CQD photovoltaic (PV) devices. A rough energy landscape has two related potential implications in PV devices; not only can it impede transport but it can also create "quantum traps" in which the presence of a small-bandgap inclusion could lead to enhanced recombination.

We begin with a brief discussion of the quantum dot films employed in our devices. Ideally, a quantum dot solid will possess a pristine bandgap free of smaller-bandgap inclusions. Under illumination, a device at open-circuit conditions will achieve an open-circuit voltage defined by, and approximately 0.35 eV less than, that bandgap.[15] When a smaller-bandgap inclusion is incorporated (Figure 1a), but the concentration of the inclusion is less than that of the majority matrix, the majority-carrier band (valence band in Figure 1a) will be

Received: November 26, 2011
Revised: January 6, 2012
Published: January 18, 2012

dx.doi.org/10.1021/nl2041589 | *Nano Lett.* 2012, 12, 1007−1012

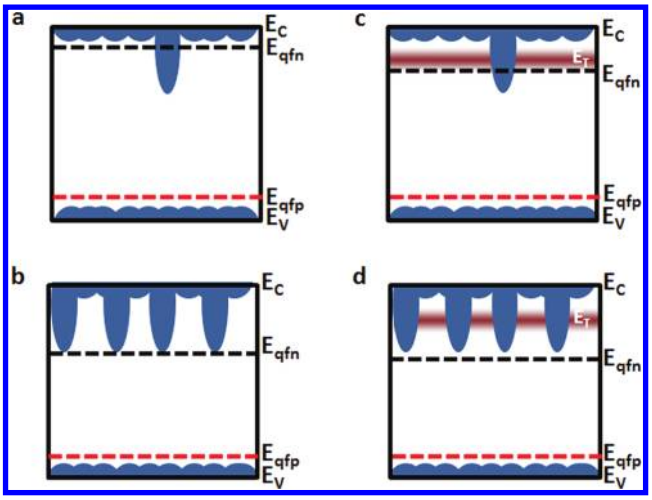

Figure 1. Schematic of the energy bands in quantum dot films (a) comprised of predominantly a single size of CQDs with a small addition of a smaller bandgap CQD; (b) possessing many inclusions of small bandgap CQDs; (c) dominated by a trap density near the conduction band; and (d) affected by both traps and substantial small-bandgap inclusions. E_{qfn} and E_{qfp} signify the electron and hole quasi-Fermi levels respectively. E_c and E_v are the quantum-confined conduction and valence band energies.

minimally affected,[16] and the minority-carrier band (conduction band in Figure 1a) will see a quantum trap of energetic depth equal to the bandgap difference between the inclusion and the matrix. Presumably some density of such defects can be tolerated with minimal impact. Above some threshold density (Figure 1b), photocarriers will fill the inclusions predominantly, and the open-circuit voltage will become determined, or pinned,[17] by the inclusions instead of the matrix.

We designed a simple experiment to explore this concentration threshold. We generated controlled mixtures of quantum dots in a known ratio of small diameter, large bandgap (matrix) nanoparticles to large diameter, small bandgap (inclusion, quantum trap) nanoparticles. We built strongly electronically coupled quantum dot films through a previously reported solid-state replacement of long oleic acid with short mercaptopropionic acid.[9]

As expected, the photoluminescence (PL) spectra of the large-diameter-doped quantum dot films showed the emergence of a long-wavelength peak that grew at the expense of the shorter-wavelength peak as the inclusion concentration was increased (Figure 2a). More specifically, the ratio between the long-wavelength peak and short-wavelength peak increased with increasing inclusion concentration. Even when only 1% of the inclusions were doped into the matrix, the luminescence feature associated with the inclusions dominated. This is consistent with efficient transfer of exciton from the primary light-absorbers (the small-diameter quantum dots) to the minority smaller-bandgap inclusions. Such transfer to the smallest bandgap moiety has been previously observed.[18−20] It is consistent with the efficient dot-to-dot transfer of photocarriers necessary to achieve the high short-circuit photocurrents (20 mA/cm^2) observed in CQD photovoltaic devices.[8,21] Figure 2b shows PL for the 0% inclusion case (i.e., a pure phase of small diameter CQDs) and the 100% inclusion case (i.e., large diameter CQDs only) to indicate that the PL quantum efficiency of the two CQD sizes is of the same order.

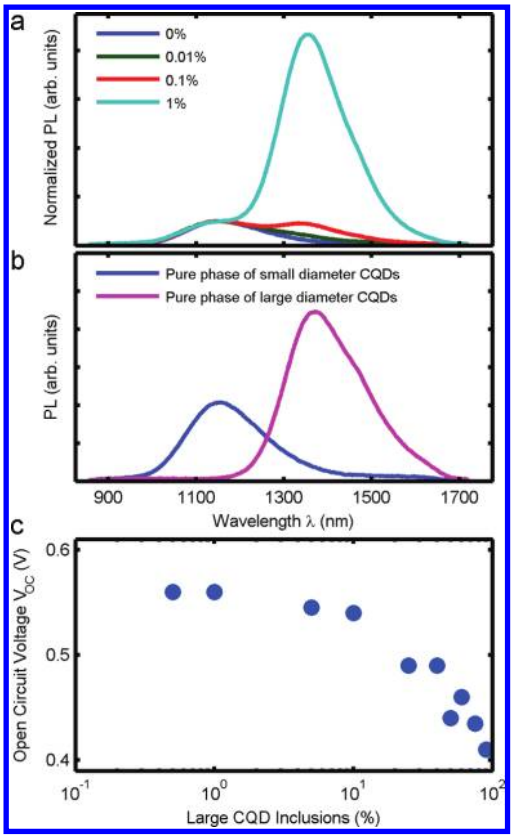

Figure 2. (a) Photoluminescence of films with varying percentages of large diameter inclusions. All spectra are MPA-ligand-treated and are normalized to the 0% short-wavelength peak at ∼1150 nm. This normalization reveals the ratio of the long-wavelength peak relative to the short-wavelength peak. (b) Photoluminescence spectra of small diameter (0%) and large diameter (100%) CQD films. The spectra are not normalized and reveal the quantitative ratio of luminescence efficiencies for the two constituent populations of dots reported in (a). (c) Open circuit voltage of solar cells as a function of the concentration of small bandgap inclusions. The *x*-axis is presented on a logarithmic scale to highlight the low-inclusion−concentration regime.

We also constructed photovoltaic devices using these same quantum dot films. We built depleted-heterojunction devices similar to those previously reported.[9] We summarize in Figure 2c the dependence of open circuit voltage (V_{oc})on inclusion concentration. Below 1% doping, no observable impact is seen. A modest loss of ∼10−20 mV is seen up to 10% doping. Only at even higher doping levels is a major decrease in open-circuit voltage seen.

We were struck with the fact that the concentration threshold at which PL became inclusion-dominated (1%) was vastly lower than the concentration threshold at which open-circuit voltage became significantly degraded (10%). We had initially expected that once small-gap quantum dots dominated luminescence they would also limit the quasi-Fermi level separation and thus the V_{oc}.

Recently, a role for surface traps in the photovoltaic performance of CQD PV devices has been presented and substantiated using time-resolved infrared spectroscopy.[8] If such traps were present in significant proportions in our CQD films and did not possess strong luminescence of their own, they could be the primary agents responsible for limiting the V_{oc}.[22] Only when the small-gap CQD inclusion density reached

dx.doi.org/10.1021/nl2041589 | *Nano Lett.* 2012, 12, 1007−1012

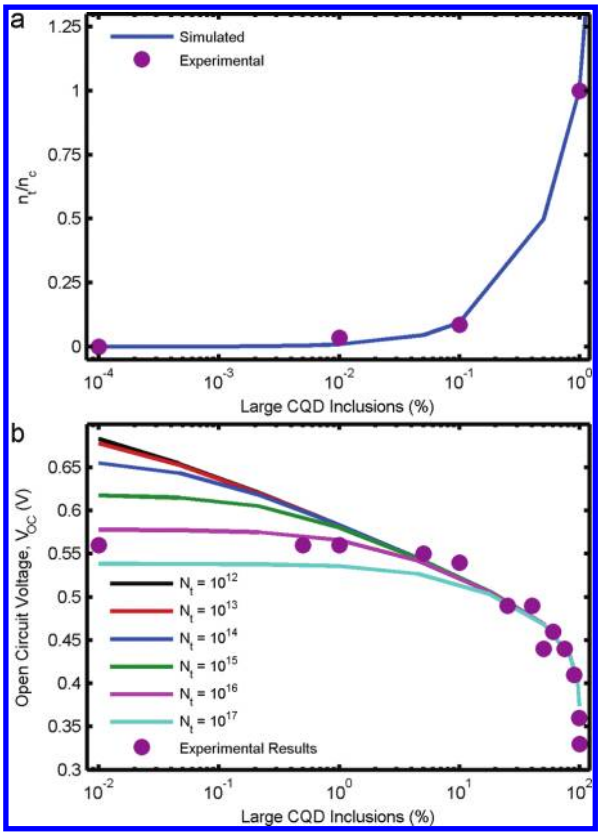

Figure 3. (a) Carrier occupation and thus recombination potential calculated both experimentally and from simulation in films of mixed quantum dots, experimental metrics extracted from Figure 2a and plotted as circles. (b) V_{OC} as a function of large diameter, small bandgap CQD inclusions for different trap densities (N_t), each with a depth of 0.25 eV below the conduction band edge. Experimental results from Figure 2c are also plotted as purple circles.

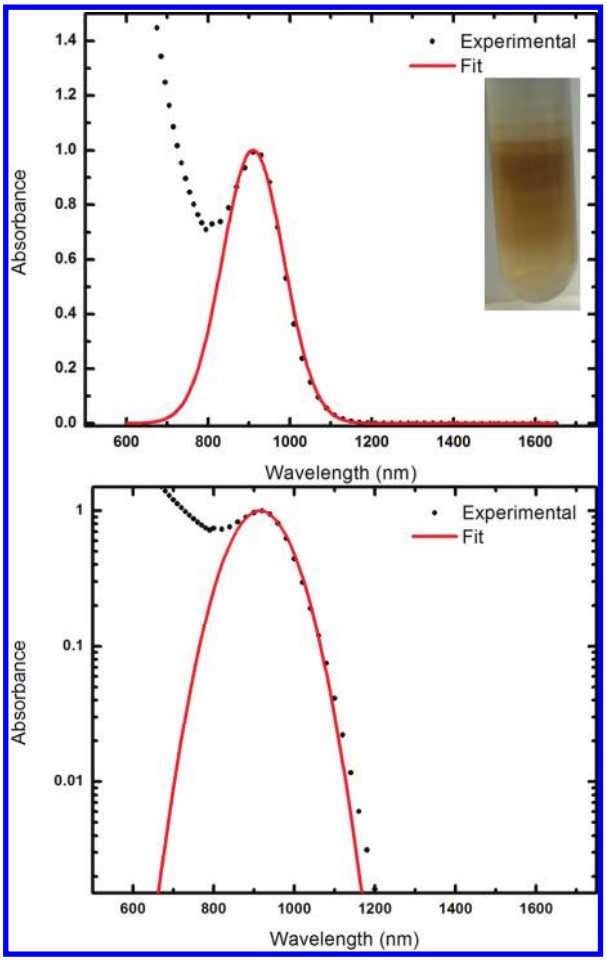

Figure 4. (a) Solution absorption spectrum of 1.3 eV CQDs fitted with a Gaussian (inset) centrifuge tube showing the ultracentrifugation capabilities of separating out different CQD size bands. (b) Same absorption spectrum with the *y*-axis scaled logarithmically, allowing for a better Gaussian fit.

a very high threshold would the inclusions limit V_{oc}. Well before this concentration, the small-gap inclusions could nevertheless contain vastly more photocarriers than the small diameter CQD matrix, accounting for the emergence of predominant PL prior to V_{OC} loss. Within this scenario, photocarriers can exist at either the small diameter CQD bandedge, the large diameter CQD bandedge, or in surface traps. Those in surface traps will not recombine radiatively, while those at the band edges will. The PL spectrum, therefore, only probes the relative populations of the states associated with the presumed radiative band-to-band recombination, while not explicitly revealing the nonradiative process.

We turned to numerical modeling (Supporting Information S1) to provide a quantitative picture of this phenomenon. We account for both inclusions and surface traps in this model, a situation depicted in Figure 1c (surface traps dominate E_{qfn}) and 1d (small-gap inclusions dominate E_{qfn}).

As seen in Figure 3b, we are able to predict the observed dependence of V_{oc} on inclusion density if we let surface traps exhibit an energy depth 0.25 eV below the quantum-confined conduction band-edge. This choice is consistent with recent reports for PbS,[8] but of course is not universal and will depend on the ligand, the quantum-confined bandgap, and the choice of quantum dot material composition. We modeled the small-gap inclusions as 0.35 eV deep traps, an amount equal to the bandgap difference between the matrix and inclusions we employed in our experiments. A surface trap density of $\sim 10^{16}$ cm^{-3} led to the best agreement with the experimentally observed dependence of V_{oc} on inclusion density.

We were also able to explain, using the same choice of surface trap state density and energy, the dependence of the ratio of small-gap (inclusion) to large-gap (matrix) PL intensity (Figure 3a). Here we used the quasi-Fermi level position predicted by the simulator under standard illumination conditions to obtain the ratio of photocarriers in the inclusions to photocarriers in the quantum-confined conduction band levels (Supporting Information S2). We plot this photocarrier ratio $R = n_t/n_c$ and find that it predicts the luminescence ratio well.

These results lend credence to this simple model that includes the effects of both surface traps and small-gap inclusions. The method of doping using inclusions also provides a convenient experimental technique for investigating whether one is in the polydispersity-limited regime or not. Our results immediately suggest that typical CQD solids, which employ nanoparticles having inhomogeneous linewidths of 100−150 meV, are likely not polydispersity-limited in their performance.

We then sought to explore within this model the implications on device performance of realistic CQD size distributions. We expected that a Gaussian size distribution would adequately

dx.doi.org/10.1021/nl2041589 | *Nano Lett.* 2012, 12, 1007−1012

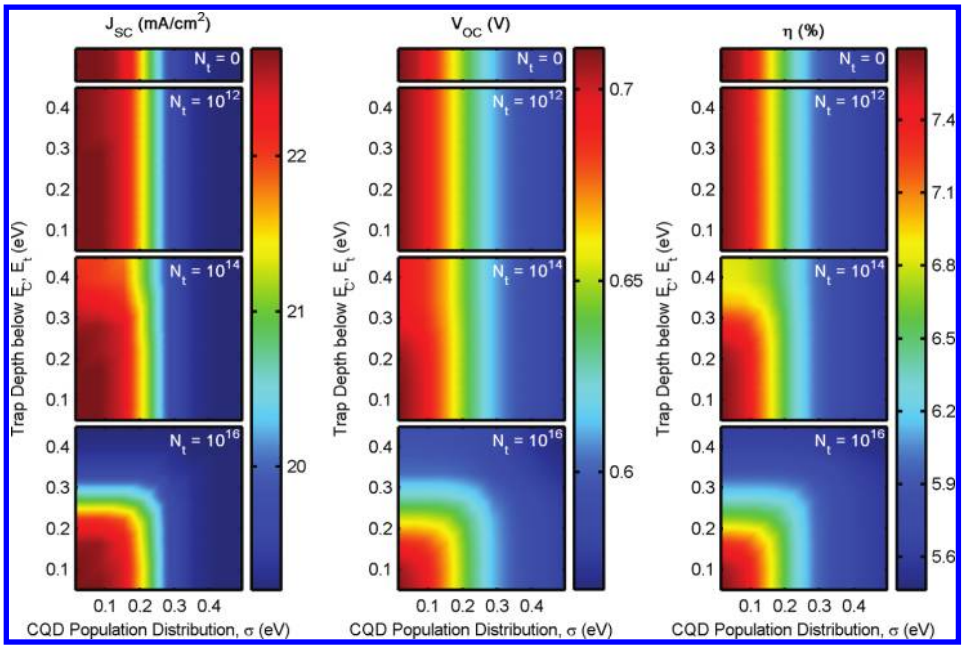

Figure 5. Modeled device performance for varying trap densities (N_t varies by row of graph and is indicated on each plot) as a function of trap depth (E_t) and the CQD population distribution broadness (σ). The left column represents the short circuit current density (J_{SC}), the middle column represents the open circuit voltage (V_{OC}), and the right column represents the power conversion efficiency, η.

model our observed absorption spectrum and wished to verify this experimentally first. Naturally there exists a homogeneous component to line width as well. Prior results suggest that the homogeneous line width is small compared to inhomogeneous ones, especially for the case of highly confined quantum dot systems.[23] A solution of the quantum dots used herein that had undergone layered-solvent ultracentrifugation[24] forms discrete bands of color (Figure 4a, inset), also consistent with an appreciable role for nanoparticle diameter distribution.

Figure 4 shows a solution-phase absorption spectrum of CQDs centered at 1.3 eV plotted on both linear and logarithmic curves (see Supporting Information S3 for high-dynamic-range absorption measurement methodology). We fit the spectrum using a Gaussian function. From the standard deviation (σ) of Figure 4b, which provides a more accurate fit that resolves the low-energy spectrum, combined with published wavelength-size dependence,[16] we extract a size and size distribution of 3.6 ± 0.3 nm, which is in agreement with prior reports based on microscopy.[25]

We therefore pursued modeling of the impacts on device performance of polydispersity using a Gaussian model of quantum dot size distribution (Supporting Information S4). Figure 5 shows the dependence of short circuit current density (J_{SC}), V_{oc}, and solar power conversion efficiency (η) on both surface trap density (vertical axes) and the standard deviation of the quantum dot bandgap distribution.

The transition between surface-trap-dominated to polydispersity-dominated performance lies along the diagonals at which the density and energy depth of each are comparable. As seen in our experiments above, present-day devices with their typical quantum dot bandgap standard deviations in the range 100−150 meV are dominated in reality by surface traps and see marginal benefit from reduction in polydispersity.

Future devices with well-passivated CQDs will benefit from reduced polydispersity; once surface traps are more fully addressed in quantum dot solids, achieving polydispersities of 50 meV or less will lead to device performance that sees very little harmful impact from polydispersity. Since this is achievable using careful synthesis, size-selective precipitation, and, if necessary, density-gradient ultracentrifugation, this finding is encouraging for continued progress in CQD PV efficiency.

Methods. One-dimensional models were prepared using SCAPS 3.0.00 employing CQD absorption coefficients and doping densities based on measured values. Electron affinities were based on literature values.[16] Trap depths are 0.25 eV below the conduction band edge except where explicitly stated.

PbS colloidal quantum dots were synthesized using a variation on a literature method.[26] TiO_2 electrodes were prepared from a sol−gel solution[27] on SnO_2/F-coated glass substrates (Pilkington TEC 15, Hartford Glass, Inc.). CQD films were prepared on TiO_2 electrodes by multilayer spincoating of 50 mg mL^{-1} solution in octane under ambient conditions. Each layer was deposited at 2500 rpm and treated briefly with 10% 3-mercaptopropionic acid in methanol also spin-cast at 2500 rpm; each layer was then rinsed with methanol while spinning at 2500 rpm. Each device consisted of eight layers with each layer being approximately 25 nm resulting in a total device thickness of ∼200 nm. The device thickness has been previously calibrated using cross-sectional SEM measurements.[8,9,18,21,27] The device was then transferred to a glovebox with N_2 atmosphere and left overnight. Contacts consisting of 10 nm of MoO_3, followed by 15 nm of gold topped with 110 nm of silver were deposited by thermal and electron beam evaporation at rates of 0.2 (thermal), 0.4 (electron beam), and 1 Å/s (thermal), respectively, at a pressure of $<1 \times 10^{-6}$ mbar. Contact sizes were 0.061 cm^2.

J−*V* data was measured using a Keithley 2400 source-meter under ambient conditions. The solar spectrum at AM1.5 was simulated to within class A specifications (less than 25% spectral mismatch) with a Xe lamp and filters (ScienceTech) with measured intensity at 100 mW cm^{-2}. The source intensity was measured with a Melles-Griot broadband power meter (responsive from 300 to 2000 nm), through a circular 0.049

dx.doi.org/10.1021/nl2041589 | *Nano Lett.* 2012, 12, 1007−1012

cm^2 aperture at the position of the sample and confirmed with a calibrated solar cell (Newport, Inc.). The accuracy of the current−voltage measurements was estimated to be ±7%.

Absorption spectra were acquired using a Cary 500 UV−vis-IR Scan spectrometer operating in transmission mode. Photoluminescence experiments were carried out using an Ocean Optics NIR512 spectrometer coupled to a focusing lens and 900 nm long pass filter through an optical fiber while simultaneously illuminating the sample with a HeNe 633 nm continuous wave laser source. PL samples were prepared on plain glass substrates.

Ultracentrifugation was carried out in a Sorvall WX Ultra 90 ultracentrifuge, using a Surespin 630 rotor and polypropylene tubes. 200 μL of a CQD solution in hexane (~5 mg/ml) was layered (in the tube) on top of a liquid of an approximately linear density gradient ranging from hexane(90%)/chloroform(10%), near the top of the tube, to 100% chloroform at the bottom of the tube.

■ ASSOCIATED CONTENT

Ⓢ Supporting Information

Discussion, equations, and figures. This material is available free of charge via the Internet at http://pubs.acs.org.

■ AUTHOR INFORMATION

Corresponding Author

*E-mail: ted.sargent@utoronto.ca.

Author Contributions

§These authors contributed equally to this work.

■ ACKNOWLEDGMENTS

This publication is based in part on work supported by Award No. KUS-11-009-21 made by King Abdullah University of Science and Technology (KAUST), by the Ontario Research Fund Research Excellence Program, by the Natural Sciences and Engineering Research Council (NSERC) of Canada, and by Angstrom Engineering and Innovative Technology. D.Z., I.J.K., and R.D. acknowledge the financial support through the NSERC CGS D Scholarship, the Ontario Graduate Scholarship and the MITACS Elevate Strategic Fellowship, respectively. The authors would also like to acknowledge the technical assistance and scientific guidance of L. Brzozowski, E. Palmiano, R. Wolowiec, D. Kopilovic, and S. Hoogland.

■ REFERENCES

(1) Sargent, E. H. Infrared Quantum Dots. *Adv. Mater.* **2005**, *17*, 515−522.

(2) Konstantatos, G.; Howard, I.; Fischer, A.; Hoogland, S.; Clifford, J.; Klem, E.; Levina, L.; Sargent, E. H. Ultrasensitive Solution-cast Quantum Dot Photodetectors. *Nature* **2006**, *442*, 180−183.

(3) Clifford, J. P.; Konstantatos, G.; Johnston, K. W.; Hoogland, S.; Levina, L.; Sargent, E. H. Fast, Sensitive and Spectrally Tuneable Colloidal-quantum-dot Photodetectors. *Nat. Nanotechnol.* **2009**, *4*, 40−44.

(4) Colvin, V. L.; Schlamp, M. C.; Alivisatos, A. P. Light-emitting Diodes Made from Cadmium Selenide Nanocrystals and a Semiconducting Polymer. *Nature* **1994**, *370*, 354−357.

(5) Tessler, N.; Medvedev, V.; Kazes, M.; Kan, S.; Banin, U. Efficient Near-Infrared Polymer Nanocrystal Light-Emitting Diodes. *Science* **2002**, *295*, 1506−1508.

(6) McDonald, S. A.; Konstantatos, G.; Zhang, S.; Cyr, P. W.; Klem, E. J. D.; Levina, L.; Sargent, E. H. Solution-processed PbS Quantum Dot Infrared Photodetectors and Photovoltaics. *Nat. Mater.* **2005**, *4*, 138−142.

(7) Johnston, K. W.; Pattantyus-Abraham, A. G.; Clifford, J. P.; Myrskog, S. H.; MacNeil, D. D.; Levina, L.; Sargent, E. H. Schottky-quantum Dot Photovoltaics for Efficient Infrared Power Conversion. *Appl. Phys. Lett.* **2008**, *92*, 151115−3.

(8) Tang, J.; Kemp, K. W.; Hoogland, S.; Jeong, K. S.; Liu, H.; Levina, L.; Furukawa, M.; Wang, X.; Debnath, R.; Cha, D.; et al. Colloidal-quantum-dot Photovoltaics Using Atomic-ligand Passivation. *Nat. Mater.* **2011**, *10*, 765−771.

(9) Pattantyus-Abraham, A. G.; Kramer, I. J.; Barkhouse, A. R.; Wang, X.; Konstantatos, G.; Debnath, R.; Levina, L.; Raabe, I.; Nazeeruddin, M. K.; Grätzel, M.; et al. Depleted-Heterojunction Colloidal Quantum Dot Solar Cells. *ACS Nano* **2010**, *4*, 3374−3380.

(10) Coe, S.; Woo, W.-K.; Bawendi, M.; Bulovic, V. Electroluminescence from Single Monolayers of Nanocrystals in Molecular Organic Devices. *Nature* **2002**, *420*, 800−803.

(11) Klimov, V. I.; Mikhailovsky, A. A.; Xu, S.; Malko, A.; Hollingsworth, J. A.; Leatherdale, C. A.; Eisler, H.-J.; Bawendi, M. G. Optical Gain and Stimulated Emission in Nanocrystal Quantum Dots. *Science* **2000**, *290*, 314−317.

(12) Talapin, D. V.; Murray, C. B. PbSe Nanocrystal Solids for N- and p-Channel Thin Film Field-Effect Transistors. *Science* **2005**, *310*, 86−89.

(13) Liu, Y.; Gibbs, M.; Puthussery, J.; Gaik, S.; Ihly, R.; Hillhouse, H. W.; Law, M. Dependence of Carrier Mobility on Nanocrystal Size and Ligand Length in PbSe Nanocrystal Solids. *Nano Lett.* **2010**, *10*, 1960−1969.

(14) Murray, C. B.; Norris, D. J.; Bawendi, M. G. Synthesis and Characterization of Nearly Monodisperse CdE (E = Sulfur, Selenium, Tellurium) Semiconductor Nanocrystallites. *J. Am. Chem. Soc.* **1993**, *115*, 8706−8715.

(15) Henry, C. H. Limiting Efficiencies of Ideal Single and Multiple Energy Gap Terrestrial Solar Cells. *J. Appl. Phys.* **1980**, *51*, 4494.

(16) Hyun, B.-R.; Zhong, Y.-W.; Bartnik, A. C.; Sun, L.; Abruña, H. D.; Wise, F. W.; Goodreau, J. D.; Matthews, J. R.; Leslie, T. M.; Borrelli, N. F. Electron Injection from Colloidal PbS Quantum Dots into Titanium Dioxide Nanoparticles. *ACS Nano* **2008**, *2*, 2206−2212.

(17) Nagpal, P.; Klimov, V. I. Role of Mid-gap States in Charge Transport and Photoconductivity in Semiconductor Nanocrystal Films. *Nat. Commun.* **2011**, *2*, 486.

(18) Kramer, I. J.; Levina, L.; Debnath, R.; Zhitomirsky, D.; Sargent, E. H. Solar Cells Using Quantum Funnels. *Nano Lett.* **2011**, *11*, 3701−3706.

(19) Klar, T. A.; Franzl, T.; Rogach, A. L.; Feldmann, J. Super-Efficient Exciton Funneling in Layer-by-Layer Semiconductor Nanocrystal Structures. *Adv. Mater.* **2005**, *17*, 769−773.

(20) Xu, F.; Ma, X.; Haughn, C. R.; Benavides, J.; Doty, M. F.; Cloutier, S. G. Efficient Exciton Funneling in Cascaded PbS Quantum Dot Superstructures. *ACS Nano* **2011**, *5*, 9950−9957.

(21) Barkhouse, D. A. R.; Debnath, R.; Kramer, I. J.; Zhitomirsky, D.; Pattantyus-Abraham, A. G.; Levina, L.; Etgar, L.; Grätzel, M.; Sargent, E. H. Depleted Bulk Heterojunction Colloidal Quantum Dot Photovoltaics. *Adv. Mater.* **2011**, *23*, 3134−3138.

(22) Kramer, I. J.; Sargent, E. H. Colloidal Quantum Dot Photovoltaics: A Path Forward. *ACS Nano* **2011**, *5* (11), 8506−8514.

(23) Wise, F. W. Lead Salt Quantum Dots: The Limit of Strong Quantum Confinement. *Acc. Chem. Res.* **2000**, *33*, 773−780.

(24) Carney, R. P.; Kim, J. Y.; Qian, H.; Jin, R.; Mehenni, H.; Stellacci, F.; Bakr, O. M. Determination of Nanoparticle Size Distribution Together with Density or Molecular Weight by 2D Analytical Ultracentrifugation. *Nat. Commun.* **2011**, *2*, 335.

(25) Ihly, R.; Tolentino, J.; Liu, Y.; Gibbs, M.; Law, M. The Photothermal Stability of PbS Quantum Dot Solids. *ACS Nano* **2011**, *5*, 8175−8186.

(26) Hines, M. A.; Scholes, G. D. Colloidal PbS Nanocrystals with Size-Tunable Near-Infrared Emission: Observation of Post-Synthesis Self-Narrowing of the Particle Size Distribution. *Adv. Mater.* **2003**, *15*, 1844−1849.

(27) Liu, H.; Tang, J.; Kramer, I. J.; Debnath, R.; Koleilat, G. I.; Wang, X.; Fisher, A.; Li, R.; Brzozowski, L.; Levina, L.; et al. Electron

Acceptor Materials Engineering in Colloidal Quantum Dot Solar Cells.
Adv. Mater. **2011**, *23*, 3832−3837.